Ocean Sci. Discuss., 8, 613–638, 2011
www.ocean-sci-discuss.net/8/613/2011/
doi:10.5194/osd-8-613-2011

Ocean Science Discussions

Quality control of automated hyperspectral remote sensing measurements from a seaborne platform

S. P. Garaba[1,2], M. R. Wernand[3], and O. Zielinski[2]

[1]University of Bremen, Department of Geosciences, P.O. Box 330440, 28334 Bremen, Germany
[2]Institute of Marine Resources, Department of Marine Physics and Sensors, Bussestraße 27, 27570 Bremerhaven, Germany
[3]Royal Netherlands Institute for Sea Research, Physical Oceanography, Marine Optics & Remote Sensing, P.O. Box 59, 1790AB Den Burg, Texel, The Netherlands

Received: 28 December 2010 – Accepted: 18 March 2011 – Published: 30 March 2011

Correspondence to: S. P. Garaba (s_yninm5@uni-bremen.de)

Published by Copernicus Publications on behalf of the European Geosciences Union.

Quality control of automated hyperspectral measurements

S. P. Garaba et al.

Abstract

In this study four data quality flags are presented for automated and unmanned above-water hyperspectral optical measurements collected underway in the North Sea, The Minch, Irish Sea and Celtic Sea in April/May 2009. Coincident to these optical measurements a DualDome D12 (Mobotix, Germany) camera system was used to capture sea surface and sky images. The first three flags are based on meteorological conditions, to select erroneous incoming solar irradiance (E_S) taken during dusk, dawn, before significant incoming solar radiation could be detected or under rainfall. Furthermore, the relative azimuthal angle of the optical sensors to the sun is used to identify possible sunglint free sea surface zones. A total of 629 spectra remained after applying the meteorological masks (first three flags). Based on this dataset, a fourth flag for sunglint was generated by analysing and evaluating water leaving radiance (L_W) and remote sensing reflectance (R_{RS}) spectral behaviour in the presence and absence of sunglint salient in the simultaneously available sea surface images. Spectra conditions satisfying "mean L_W (700–950 nm) $< 2\,\mathrm{mW\,m^{-2}\,nm^{-1}\,Sr^{-1}}$" or alternatively "minimum R_{RS} (700–950 nm) $< 0.010\,\mathrm{Sr^{-1}}$", mask the most measurements affected by sunglint, providing efficient flagging of sunglint in automated quality control. It is confirmed that valid optical measurements can be performed $0^\circ \le \Phi \le 360^\circ$ although $90^\circ \le \Phi \le 135^\circ$ is recommended.

1 Introduction

Remote sensing has become a key tool in the investigation of marine biochemical and geophysical characteristics on a regional or global scale (IOCCG, 2000; Schofield et al., 2004; Dierssen, 2010). During the last few decades, technical progress in remote sensing has made it possible to carry out optical measurements from in-water, above-water, airborne and satellite platforms (Moore et al., 2009). However, automated and unmanned optical measurements from any of these platforms are likely to be erroneous

OSD

8, 613–638, 2011

due to meteorological conditions (e.g. rainfall, cloud cover, humidity, and dusk/dawn conditions), sunglint, and sensor setup (Gordon and Jacobs, 1977; Wernand, 2002; Zhang and Wang, 2010). Therefore quality control to eliminate these disturbing factors is a crucial procedure in determining colour of seawater.

Sunglint is a phenomenon resulting from a direct beam of sunlight reflected from a seawater surface directly into the down looking optical sensor (Morel and Gordon, 1980; Ottaviani et al., 2008). Studies suggest that sunglint is caused by Fresnel reflection from a number of "dancing facets" on the wind affected seawater surface and is controlled by the position of the sun, optical sensor viewing angle, water refractive index, wind direction and speed (Kay et al., 2009; Zhang and Wang, 2010). In a recent audit of sunglint correction models for optical measurements in marine environments it is conceded that despite their benefits most of these models rely partly on the black pixel assumption and therefore tend to moderately correct glint pixels (Kay et al., 2009). This black pixel assumption, water leaving radiance is insignificant in the near infra-red spectrum, has been reported to be inconsistent to some degree in coastal and turbid waters, which contributes also to the fact that correction models come with a probability of over- or underestimation of apparent and inherent optical properties (Siegel et al., 2000; Shi and Wang, 2009). This framework provides the motivation to develop a sunglint flag with the objective of masking affected data, hence minimising the probability of errors likely to occur when using correction models.

Wernand (2002) described a meteorological quality flagging method to optimise automated hyperspectral measurements for coastal and shelf seas. To minimise sunglint he suggests the use of two optical sensors looking in different azimuthal directions to measure water surface leaving radiance and utilises the lowest water surface leaving radiance for each measurement, so as to select the spectrum with the least sunglint. While this setup is useful and minimises sunglint effect on measurements, it requires additional sensors to be installed with the possible risk of sunglint still affecting both sensors.

OSD
8, 613–638, 2011

This study presents a set of four quality control flags for automated and unmanned above-water hyperspectral measurements, a flag to mask sunglint is generated here to compliment meteorological flags reported by Wernand (2002). These hyperspectral measurements are supplemented by simultaneous sky and sea surface images from a camera system. Parallel to the image and spectrum analysis, optimum azimuthal zones for sensor measurement were assessed with the goal to identify sunglint affected and non affected zones. The sea surface images act as "sea-truth" in the validation step of spectra and the Solar Position Algorithm, SPA (Reda and Andreas, 2004) generated estimate azimuthal angles of the sun during the field campaign.

In the next section, the measurement methodology will be explained followed by a presentation of the results and a discussion of the study findings. Finally, the new flagging method will be presented along with possible future developments.

2 Data and methods

Underway optical measurements in the North Sea, Scotland Sea, Irish Sea and Celtic Sea were performed aboard R/V *Heincke* cruise HE302 between 21 April and 14 May 2009. Ocean Data View (Schlitzer, 2010) was used to generate the study area map, Fig. 1, which shows the ship track for which above-water hyperspectral measurements were obtained.

2.1 Instrumentation

A RAMSES-ACC hyperspectral cosine irradiance meter (TriOS, Germany) was used to measure incoming solar radiation, E_S (λ) and two RAMSES-ARC hyperspectral radiance meters with a field-of-view of 7° in air, were used to detect respectively the sea surface radiance L_{sfc} $(\theta_{sfc}, \Phi, \lambda)$ and sky radiance L_{sky} $(\theta_{sky}, \Phi, \lambda)$. A frame (see Fig. 2) designed to hold the irradiance sensor facing upwards, the sky and sea surface radiance sensors at zenith angels $\theta_{sfc} = 45^\circ$ and $\theta_{sky} = 135^\circ$, was fixed to the mast of the ship facing the starboard, 12 m above sea surface. These spectral measurements were automatically collected at 15 min intervals over a spectral range $\lambda = 320$–950 nm in steps of 5 nm. Spectrum classification, visible (VIS), $\lambda = 320$–700 nm, and near infrared (NIR), $\lambda = 700$–950 nm, was implemented.

A DualDome D12 (Mobotix, Germany) camera system with customised lense objective L43 with a field-of-view of 45°, was used to capture simultaneous images of the sky and sea surface during hyperspectral measurements as illustrated in Fig. 2. The positioning height of the camera system and optical sensors proved to be unaffected by sea spray. The ship's position and heading were recorded using a Differential Global Position System (DGPS) and sampling times were logged in UTC.

2.2 Methods

The first step in quality control data processing, involved implementing the meteorological flagging (Wernand, 2002) on E_S (λ) measurements using MATLAB 2010a (MathWorks, USA). The flag conditions; (1) E_S $(\lambda = 480\,\text{nm}) > 20\,\text{mW}\,\text{m}^{-2}\,\text{nm}^{-1}$ sets a threshold for which significant E_S (λ) can be measured, (2) E_S $(\lambda = 470\,\text{nm})/E_S$ $(\lambda = 680\,\text{nm}) < 1$ will mask spectra affected by dawn/dusk radiation, (3) E_S $(\lambda = 940\,\text{nm})/E_S$ $(\lambda = 370\,\text{nm}) < 0.25$ will mask spectra affected by rainfall and high humidity. E_S (λ) and corresponding L_{sfc} $(\theta_{\text{sfc}}, \Phi, \lambda)$, L_{sky} $(\theta_{\text{sky}}, \Phi, \lambda)$ measurements that passed this meteorological flagging were then used to derive water leaving radiance, L_W $(\theta_{\text{sfc}}, \Phi, \lambda)$, and remote sensing reflectance, R_{RS} (θ, Φ, λ) according to Eq. (1) (Mueller et al., 2003);

$$R_{RS} = \frac{L_W}{E_S} = \frac{L_{\text{sfc}} - \left(\rho_{\text{air-sea}} \cdot L_{\text{sky}}\right)}{E_S} \tag{1}$$

where $\rho_{\text{air-sea}}$ is the air-sea interface reflection coefficient which is dependent on cloud cover, sensor viewing angle, and wind speed. It has been reported that for measurements L_{sky} $(\lambda = 750\,\text{nm})/E_S(\lambda = 750\,\text{nm}) \geq 0.05$, $\rho_{\text{air-sea}} = 0.0256$ is suitable, also consistent with the available collected spectra (Ruddick et al., 2006). The radiometric

OSD
8, 613–638, 2011

Quality control of automated hyperspectral measurements

S. P. Garaba et al.

optical measurements used and computed in Eq. (1) are available on PANGAEA (Garaba et al., 2010a, b, c, d).

2.2.1 Sunglint flag

The derived L_W and R_{RS} from Eq. (1) were utilised in the testing and evaluation of the new sunglint flag intended to mask measurements affected by sunglint. Parallel to this investigation, the SPA and DGPS data were utilised along with Eq. (2) as complimentary tools to derive the relative angle of the optical sensors to the sun's azimuth position, Φ_{derived};

$$\Phi_{\text{derived}} = \left(\Phi_{\text{sun}} - \left(\Phi_{\text{ship}} + \Phi_{\text{sensor}}\right)\right) \text{ modulo } 360^\circ \tag{2}$$

where Φ_{sun} is the sun's azimuthal position, Φ_{ship} ship's azimuthal heading, and the sensor azimuthal heading $\Phi_{\text{sensor}} = 85^\circ$. In order to maintain the circular nature of angle $0^\circ \leq \Phi_{\text{derived}} \leq 360^\circ$, the modulo arithmethic was applied. A test was then performed on Φ_{derived}, using corresponding sea surface images as "sea truth", to identify the number of optical measurements consistent with $90^\circ \leq \Phi \leq 135^\circ$ (Fougnie et al., 1999; Mueller et al., 2003; Deschamps et al., 2004). This test was also aimed to answer: is it possible to obtain useful optical measurement from an automated and unmanned seaborne platform for $0^\circ \leq \Phi_{\text{derived}} < 90^\circ$ and $135^\circ < \Phi_{\text{derived}} \leq 360^\circ$?

The sunglint flag was developed on the premise that water absorbs light in the NIR, but reflects light due to a wind roughened sea surface and/or scattering influenced by optically active water constituents. In Fig. 3 a simplified activity diagram illustrates the steps that were implemented in this sunglint flag investigation and evaluation;

1. Sea surface images were retrieved, matching the unmasked spectra validated with the meteorological flagging (Wernand, 2002), visually inspected and classified into; Nns – image set without sunglint or Ns – image set with sunglint,

2. Analysis of the two sets Nns and Ns was now focussed on identifying unique characteristics using L_W and R_{RS}. It involved looking at individual spectra and

OSD
8, 613–638, 2011

mean spectra for the two sets over the whole spectrum range ($\lambda = 320$–950 nm), to obtain a general overview on typical spectra for set Nns and Ns,

3. The goal of this step was to eliminate spectra with images in Ns while conversely retaining as much as possible spectra in Nns. Hence utilising the findings from step 2, i.e. spectrum shape, behaviour and magnitude variations of both L_W and R_{RS} in the VIS and NIR, a combination of inequality equations and band ratios were implemented to assess and generate the sunglint flag;

   – first evaluation test used the NIR mean values for set Nns and Ns to obtain threshold values specific to each set, this test was then repeated using the minimum values in the NIR,

   – next test involved using the classical band ratioing based on dominant spectral bands both in the VIS and NIR i.e. $\lambda = 400$ nm, 460 nm, 760 nm, 940 nm (Halthore et al., 1997; Wernand, 2002; Kay et al., 2009).

4. In the last step the sunglint flag was produced after quality and quantity control check from step 3.

3 Results and discussion

In the previous section the methods used in spectra measurement during the field campaign were explained and in this section the new proposed quality control will be presented along with other findings. A total of 629 spectra measurements satisfied the test conditions of the meteorological flagging. Sea surface image assessment of these corresponding to the unmasked 629 spectra, revealed 501 images free of sunglint, Nns and 128 images affected by sunglint, Ns.

OSD
8, 613–638, 2011

3.1 Sunglint image analysis

Automated and unmanned optical measurements from a seaborne platform are challenging. It is difficult to adhere to recommended sensor setups for θ_{sfc}, θ_{sky}, Φ; thus inevitable to collect erroneous measurements affected by sunglint, whitecap and foam (Gordon, 1985; Moore et al., 1998; Fougnie et al., 1999; Hooker and Morel, 2003; Kay et al., 2009). In this study, underway measurements were made aboard R/V *Heincke* on the track illustrated in Fig. 1. Figure 4 demonstrates typical sources of error, revealed by the image inspection in step 2 of Fig. 3. The image inspection was performed by two investigators with an additional referee. Main sources of contamination were identified as sunglint, whitecaps and foam, the latter two resulting in similar sunlight influenced spectral patterns.

3.2 Sunglint flag

The assessment of the spectra from the sample sets Nns and Ns indicated that R_{RS} (NIR) and L_W (NIR) were significantly higher in the presence of sunglint. L_W values over the whole measured spectrum, $\lambda = 320$–950 nm, were higher for the set Ns relative to set Nns in both VIS and NIR ranges. R_{RS} values were enhanced for the set Ns compared to set Nns. In Fig. 5 normalised sample mean spectra shapes for Nns (501 spectra) and Ns (128 spectra) are presented to illustrate the aforesaid findings. Data normalisation was applied to maintain the spectral shape while simplifying comparison of spectra, dividing each L_W and R_{RS} measurement by the maximum value for each measurement. However, for determining the new flag, the actual computed spectral measurements L_W and R_{RS} were used.

The mean Ns spectrum in Fig. 5 shows normL_W and normR_{RS} values elevated by sunglint compared to mean Nns spectrum. To further investigate and understand sunglint spectral characteristics, 13 of the 128 sea surface images in Ns were identified to be completely affected by sunglint and in Fig. 6 their spectral shapes reveal the same trend shown in Fig. 5. The findings confirm that in the presence of sunglint,

Discussion Paper | Discussion Paper | Discussion Paper | Discussion Paper |
OSD
8, 613–638, 2011
Quality control of automated hyperspectral measurements
S. P. Garaba et al.

sea water will reflect light due to a wind roughened sea surface, evident in the sea surface images, and/or multiple scattering by optically active water constituents. This was a unique characteristic in both L_W and R_{RS} for optical measurements from this study which aided in developing the new sunglint flag.

Spectral band ratioing, a classical method in quantitative colour of seawater interpretation that is known to reveal diversity in R_{RS} shapes of seawater surface features (Lee and Carder, 2000), was implemented to help reveal the differences in Nns and Ns. The spectral bands used include; oxygen absorption band ($\lambda \approx 760$ nm) which has been used in a prior sunglint correction model (Kutser et al., 2009), precipitable water vapour absorption band ($\lambda \approx 940$ nm) known to interact with solar radiation in the NIR among other greenhouse gases e.g. methane or carbon (Halthore et al., 1997; Kleidman et al., 2000), chromophoric dissolved organic material absorption from UV to visible, here investigated at ($\lambda \approx 400$ nm) and ($\lambda \approx 460$ nm) contribute to sunglint through particulate multiple scattering (Bricaud et al., 1981; Gallegos et al., 1990).

To summarise and evaluate the tests implemented in obtaining the best sunglint flag/mask Table 1 was generated. A ranking was introduced so as to order the methods according to their performance when eliminating or selecting the most sunglint affected measurements.

The methods in Table 1 provide an easy and simplified evaluation procedure because they include basic mathematical operations; division and inequalities. The threshold criteria was, chosen because it is a widely used technique in developing flagging and validation algorithms e.g. (Lavender et al., 2005), performed by iterative testing, i.e. first using mean values as threshold for sets Nns and Ns and then adjusting to obtain better performance. Adjusting these threshold values was aimed at; (i) masking/eliminating as many measurements in the sunglint affected set Ns, and (ii) unmasking/keeping as many measurements in the sunglint free set Nns. The performance test summarized in Table 1, revealed the best sunglint flag conditions; “mean $(L_W)_{NIR} < 2\,\mathrm{mW\,m^{-2}\,nm^{-1}\,Sr^{-1}}$”, at least 90% effective in sets Nns (97.21%) and Ns (91.41%) but falls short as 14 valid spectra (2.79% of Nns) were

OSD
8, 613–638, 2011
Quality control of automated hyperspectral measurements
S. P. Garaba et al.

masked and 11 erroneous spectra (8.59% of Ns) kept; or alternatively "minimum $(R_{RS})_{NIR} < 0.010\,\mathrm{Sr}^{-1}$", which despite the relatively low performance in set retaining measurements in Nns (94.01%) it however reduces the number of erroneous spectra kept after validation to 7 spectra (5.47% of Ns).

3.3 Remote sensing reflectance

In the previous section, a sunglint flag was generated which can be implemented using L_W or R_{RS}. In Table 2, the meteorological flagging (Wernand, 2002) conditions and sunglint flag conditions are conjointly presented. The first three flags rely on the incoming radiation, E_s, thus masking measurements taken during dusk or before significant incoming solar radiation can be detected (Flag 1), dawn (Flag 2), or under rainfall (Flag 3). Equation (1) is then implemented to derive water leaving radiance, L_W and remote sensing reflectance, R_{RS}, followed by the sunglint flag validation. In this study the sunglint flag was implemented using L_W (Flag 4a) because it is the first product of Eq. (1) but can be replaced by R_{RS} (Flag 4b) as summarised in Table 2. Proposing Flag 4a or Flag 4b was aimed at not limiting flagging to one remote sensing product e.g. L_W or R_{RS} only.

This proposed quality control method (meteorological and sunglint flagging) aims to eliminate erroneous spectral measurements collected from an unmanned and automated platform. When all the flags were applied to the available measurements, Flag 1–Flag 4a, a subset was selected to illustrate typical spectra for case 2 waters along the cruise track (Fig. 7).

3.4 Relative azimuth angle between the sun and the sensor

In the previous section, sunglint flags were developed using L_W and R_{RS}. Using SPA and sea surfaces images as complimentary tools, an additional evaluation based on spectra kept after running the flagging proposed in Table 2 and the matching $\Phi_{derived}$ was performed. The main goal was to answer these two questions; how many of the optical measurements of this study conform to the recommended $90^\circ \leq \Phi \leq 135^\circ$? At which Φ can valid and useful measurements be collected from an unmanned and automated platform?

According to the available measurements, valid spectra can be collected at $0^\circ \leq \Phi \leq 360^\circ$. However, the validity of the spectra is dependent on the accuracy of air-sea interface reflection coefficient estimate. Table 3 summarises these findings, it is shown that ~85% of the optical measurements at the recommended $90^\circ \leq \Phi \leq 135^\circ$ are valid. In the other regions $0^\circ \leq \Phi_{derived} < 90^\circ$ and $135^\circ < \Phi_{derived} \leq 360^\circ$ valid measurements were also collected. This can be attributed to the R/V "*pitch, roll and yaw*", also valid for ferries equipped with radiometers, motions causing fluctuations in optical sensor setup; azimuth and zenith angle changes (Mishra and Nath, 1999; Aas, 2010). The dynamic changes in the optical sensor setup on an unmanned and automated seaborne platform influence the collection of valid and invalid measurements as shown in Table 3.

4 Conclusions

Hyperspectral optical measurements from an unmanned and automated seaborne platform are often affected by meteorological conditions and sunglint. To overcome these disturbances, the new proposed sunglint flag, masks spectra affected by sunglint based on either L_W or R_{RS}, and the meteorological flags (Wernand, 2002), mask spectra affected by rainfall, dusk and dawn based on E_S to mitigate collectable erroneous measurements. A camera system, to obtain sea surface images (evidence for sunglint, whitecaps, foam) and sky images (evidence for cloud cover or overhead sun), and the SPA to estimate the azimuthal angle of the sun relative to optical sensors, can both be used as complimentary tools. Optical measurements collected as proposed in this study, e.g. the planned permanent installation of this system on R/V *Heincke*, will provide test datasets for further validation of the meteorological and sunglint flagging for different water bodies.

In this study it is assumed sunglint was the main cause of error in the collected measurements after applying the meteorological flagging (Wernand, 2002). However, the influence of whitecaps and foam has been reported to cause both; (i) a decrease in reflectance in the NIR due to radiation absorption by large air bubbles (Whitlock et al., 1982; Frouin et al., 1996), or physical coolness of residual foam (Marmorino and Smith, 2005), (ii) enhanced reflectance occurring as soon as waves break generating thick strong reflecting foam (Moore et al., 1998). Image analysis revealed that in sea surface images influenced by whitecaps/foam, sunglint was also present and it was not possible to distinguish how each contribute to the spectra. It was therefore assumed that for the available measurements sunglint and whitecaps/foam led to erroneous measurements. It is therefore important that in future studies the contribution of whitecaps and foam be specifically investigated with respect to sunglint flagging.

Automated and unmanned above-water optical measurements based on recommend optical sensor setup for example the reported $90^\circ \leq \Phi \leq 135^\circ$ (Mueller et al., 2003) cannot be completely achieved and does not guarantee valid measurements, also reported by Aas (2010). In this study it has been shown that valid measurements can be obtained for $0^\circ \leq \Phi \leq 360^\circ$ from an unmanned seaborne platform. It is recommended that prior to the automated and unmanned optical measurements the SPA be utilised to predict or identify optimal Φ despite the limiting factors of R/V "*pitch, roll and yaw*" motions. Here the idea is not to necessarily change the cruise track but to perfom underway measurements avoiding sunglint. Alternatives approaches to minimise sunglint, but increasing technical requirements, would be (a) to turn the sensors by some automatic device or (b) to have more sensors looking at different azimuthal directions. However for fixed platforms, such as piles, these altenative approaches can be avoided if SPA is utilised beforehand to limit sunglint influenced measurements. Furthermore, investigations in coastal and turbid waters using hyperspectral radiometers are still needed to fully understand the sunglint spectral signatures both in the VIS and NIR ranges.

OSD

8, 613–638, 2011

Acknowledgements. The data used in this study was collected during the North Sea Coast Harmful Algal Bloom (NORCOHAB II) field campaign onboard R/V *Heincke* cruise HE302. The authors extend their gratitude to the captain and crew of R/V *Heincke*, and to R. H. Henkel, B. Krock, B. Saworski and D. Voß for their support during the field campaign. Many thanks to D. Brockman, J. Busch, B. Mahleko, K. Nute, J. Schulz, and the two anonymous referees for their valuable input and critics. The Institute of Marine Resources (IMARE) GmbH is subsidized by European Regional Development Fund (ERDF).

References

Aas, E.: Estimates of radiance reflected towards the zenith at the surface of the sea, Ocean Sci., 6, 861–876, doi:10.5194/os-6-861-2010, 2010.

Bricaud, A., Morel, A., and Prieur, L.: Absorption by dissolved organic matter of the sea (yellow substance) in the UV and visible domains, Limnol. Oceanogr., 26, 43–53, 1981.

Deschamps, P.-Y., Fougnie, B., Frouin, R., Lecomte, P., and Verwaerde, C.: SIMBAD: A Field Radiometer for Satellite Ocean-Color Validation, Appl. Optics, 43, 4055–4069, doi:10.1364/AO.43.004055, 2004.

Dierssen, H. M.: Perspectives on empirical approaches for ocean color remote sensing of chlorophyll in a changing climate, P. Natl. Acad. Sci., 107, 17073–17078, doi:10.1073/pnas.0913800107, 2010.

Fougnie, B., Frouin, R., Lecomte, P., and Deschamps, P.-Y.: Reduction of Skylight Reflection Effects in the Above-Water Measurement of Diffuse Marine Reflectance, Appl. Optics, 38, 3844–3856, doi:10.1364/AO.38.003844, 1999.

Frouin, R., Schwindling, M., and Deschamps, P.-Y.: Spectral reflectance of sea foam in the visible and near-infrared: In situ measurements and remote sensing implications, J. Geophys. Res., 101, 14361–14371, doi:10.1029/96jc00629, 1996.

Gallegos, C. L., Correll, D. L., and Pierce, J. W.: Modeling spectral diffuse attenuation, absorption, and scattering coefficients in a turbid estuary, Limnol. Oceanogr., 35, 1486–1502, 1990.

Garaba, S., Zielinski, O., Krock, B., Henkel, R., and Voß, D.: Spectral sky radiance during the North Sea Coast Harmful Algal Bloom (NORCOHAB II) RV HEINCKE cruise HE302,

Hochschule Bremerhaven – University of Applied Sciences, doi:10.1594/PANGAEA.753832, 2010a.
Garaba, S., Zielinski, O., Krock, B., Henkel, R., and Voß, D.: Downward Irradiance during the North Sea Coast Harmful Algal Bloom (NORCOHAB II) RV HEINCKE cruise HE302, Hochschule Bremerhaven – University of Applied Sciences, doi:10.1594/PANGAEA.753830, 2010b.
Garaba, S., Zielinski, O., Krock, B., Henkel, R., and Voß, D.: Upward radiance during the North Sea Coast Harmful Algal Bloom (NORCOHAB II) RV HEINCKE cruise HE302, Hochschule Bremerhaven – University of Applied Sciences, doi:10.1594/PANGAEA.753839, 2010c.
Garaba, S., Zielinski, O., Krock, B., Henkel, R., and Voß, D.: Remote sensing reflectance during the North Sea Coast Harmful Algal Bloom (NORCOHAB II) RV HEINCKE cruise HE302, Hochschule Bremerhaven – University of Applied Sciences, doi:10.1594/PANGAEA.753840, 2010d.
Gordon, H. R.: Ship perturbation of irradiance measurements at sea. 1: Monte Carlo simulations, Appl. Optics, 24, 4172–4182, doi:10.1364/AO.24.004172, 1985.
Gordon, H. R. and Jacobs, M. M.: Albedo of the ocean-atmosphere system: influence of sea foam, Appl. Optics, 16, 2257–2260, doi:10.1364/AO.16.002257, 1977.
Halthore, R. N., Eck, T. F., Holben, B. N., and Markham, B. L.: Sun photometric measurements of atmospheric water vapor column abundance in the 940-nm band, J. Geophys. Res., 102, 4343–4352, doi:10.1029/96JD03247, 1997.
Hooker, S. B. and Morel, A.: Platform and Environmental Effects on Above-Water Determinations of Water-Leaving Radiances, J. Atmos. Ocean. Tech., 20, 187–205, doi:10.1175/1520-0426(2003)020<0187:PAEEOA>2.0.CO;2, 2003.
IOCCG: Remote sensing of ocean colour in coastal, and other optically-complex, waters, in: Reports of the International Ocean-Colour Coordinating Group, No. 3, edited by: Sathyendranath, S., Dartmouth, Canada, 140 pp., 2000.
Kay, S., Hedley, J., and Lavender, S.: Sun Glint Correction of High and Low Spatial Resolution Images of Aquatic Scenes: a Review of Methods for Visible and Near-Infrared Wavelengths, Remote Sensing, 1, 697–730, doi:10.3390/rs1040697, 2009.
Kleidman, R. G., Kaufman, Y. J., Gao, B. C., Remer, L. A., Brackett, V. G., Ferrare, R. A., Browell, E. V., and Ismail, S.: Remote sensing of total precipitable water vapor in the near-IR over ocean glint, Geophys. Res. Lett., 27, 2657–2660, doi:10.1029/1999GL011156, 2000.

Kutser, T., Vahtmäe, E., and Praks, J.: A sun glint correction method for hyperspectral imagery containing areas with non-negligible water leaving NIR signal, Remote Sens. Environ., 113, 2267–2274, doi:10.1016/j.rse.2009.06.016, 2009.
Lavender, S. J., Pinkerton, M. H., Moore, G. F., Aiken, J., and Blondeau-Patissier, D.: Modification to the atmospheric correction of SeaWiFS ocean colour images over turbid waters, Cont. Shelf Res., 25, 539–555, doi:10.1016/j.csr.2004.10.007, 2005.
Lee, Z. and Carder, K. L.: Band-Ratio or Spectral-Curvature Algorithms for Satellite Remote Sensing?, Appl. Optics, 39, 4377–4380, doi:10.1364/AO.39.004377, 2000.
Marmorino, G. O. and Smith, G. B.: Bright and dark ocean whitecaps observed in the infrared, Geophys. Res. Lett., 32, L11604, doi:10.1029/2005gl023176, 2005.
Mishra, A. K. and Nath, A. N.: Determination of satellite nadir and azimuth angles for a tilting sensor, Int. J. Remote Sens., 20, 3265–3272, doi:10.1080/014311699211318, 1999.
Moore, K. D., Voss, K. J., and Gordon, H. R.: Spectral Reflectance of Whitecaps: Instrumentation, Calibration, and Performance in Coastal Waters, J. Atmos. Ocean. Tech., 15, 496–509, doi:10.1175/1520-0426(1998)015<0496:SROWIC>2.0.CO;2, 1998.
Morel, A. Y. and Gordon, H. R.: Report of the working group on water color, Bound.-Lay. Meteorol., 18, 343–355, doi:10.1007/bf00122030, 1980.
Mueller, J. L., Davis, C., Arnone, R., Frouin, R., Carder, K., Lee, Z. P., Steward, R. G., Hooker, S., Mobley, C. D., and McLean, S.: Above-Water Radiance and Remote Sensing Reflectance Measurement and Analysis Protocols, in: Radiometric Measurements and Data Analysis Protocols Ocean Optics Protocols For Satellite Ocean Color Sensor Validation, Revision 4, Volume III, edited by: Mueller, J. L., Fargion, G. S., and McClain, C. R., Goddard Space Flight Space Center, Greenbelt, Maryland, 2003.
Ottaviani, M., Spurr, R., Stamnes, K., Li, W., Su, W., and Wiscombe, W.: Improving the description of sunglint for accurate prediction of remotely sensed radiances, J. Quant. Spectrosc. Ra., 109, 2364–2375, doi:10.1016/j.jqsrt.2008.05.012, 2008.
Reda, I. and Andreas, A.: Solar position algorithm for solar radiation applications, Sol. Energy, 76, 577–589, doi:10.1016/j.solener.2003.12.003, 2004.
Ruddick, K. G., De Cauwer, V., Park, Y. J., and Moore, G.: Seaborne measurements of near infrared water-leaving reflectance: The similarity spectrum for turbid waters, Limnol. Oceanogr., 51, 1167–1179, 2006.
Schlitzer, R.: Ocean Data View, http://odv.awi.de, 2010.
Schofield, O., Arnone, R. A., Bissett, P. W., Dickey, T. D., Davis, C. O., Finkel, Z., Oliver, M.,

and Moline, M. A.: Watercolors in the Coastal Zone: What Can We See?, Oceanography, 17, 24–31, 2004.
Shi, W. and Wang, M.: An assessment of the black ocean pixel assumption for MODIS SWIR bands, Remote Sens. Environ., 113, 1587–1597, doi:10.1016/j.rse.2009.03.011, 2009.
Siegel, D. A., Wang, M., Maritorena, S., and Robinson, W.: Atmospheric Correction of Satellite Ocean Color Imagery: The Black Pixel Assumption, Appl. Optics, 39, 3582–3591, doi:10.1364/AO.39.003582, 2000.
Wernand, M. R.: Guidelines for (ship-borne) auto-monitoring of coastal and ocean colour, Proceedings of Ocean Optics XVI: 18–22 November 2002, Santa Fe, New Mexico, USA, 13 pp., 2002.
Whitlock, C. H., Bartlett, D. S., and Gurganus, E. A.: Sea foam reflectance and influence on optimum wavelength for remote sensing of ocean aerosols, Geophys. Res. Lett., 9, 719–722, doi:10.1029/GL009i006p00719, 1982.
Zhang, H. and Wang, M.: Evaluation of sun glint models using MODIS measurements, J. Quant. Spectrosc. Ra., 111, 492–506, doi:10.1016/j.jqsrt.2009.10.001, 2010.

OSD
8, 613–638, 2011

Quality control of automated hyperspectral measurements

S. P. Garaba et al.

Table 1. A summarized evaluation of the best sunglint flag conditions ranked according to their performance in masking sunglint spectra. To check for effectiveness, the percentage E (Ns) % and E (Nns) % was derived by dividing the number of spectra masked or unmasked by each condition with the actually number of spectra in sets, sunglint set Ns – 128 spectra and non sunglint set Nns – 501 spectra. NIR refers to $\lambda = 700$–950 nm.

Sunglint flag test condition	Sunglint affected observations masked	E (Ns) %	Sunglint free observations unmasked	E (Nns) %
Minimum $(L_W)_{NIR} < 0.3\,\mathrm{mW\,m^{-2}\,nm^{-1}\,Sr^{-1}}$	123	96.09	454	90.62
Mean $(R_{RS})_{NIR} < 0.010\,\mathrm{Sr^{-1}}$	123	96.09	453	90.42
Minimum $(R_{RS})_{NIR} < 0.010\,\mathrm{Sr^{-1}}$	121	94.53	471	94.01
Minimum $(L_W)_{NIR} < 0.4\,\mathrm{mW\,m^{-2}\,nm^{-1}\,Sr^{-1}}$	119	92.97	478	95.41
Mean $(L_W)_{NIR} < 2.000\,\mathrm{mW\,m^{-2}\,nm^{-1}\,Sr^{-1}}$	117	91.41	487	97.21
Minimum $(L_W)_{NIR} < 0.5\,\mathrm{mW\,m^{-2}\,nm^{-1}\,Sr^{-1}}$	115	89.84	486	97.01
Minimum $(R_{RS})_{NIR} < 0.012\,\mathrm{Sr^{-1}}$	115	89.84	479	95.61
Mean $(R_{RS})_{NIR} < 0.015\,\mathrm{Sr^{-1}}$	112	87.50	475	94.81
L_W (940)/L_W (400) < 0.145	111	86.72	480	95.81
Mean $(L_W)_{NIR} < 2.500\,\mathrm{mW\,m^{-2}\,nm^{-1}\,Sr^{-1}}$	110	85.94	492	98.20
L_W (765)/L_W (460) < 0.290	110	85.94	477	95.21
Minimum$(R_{RS})_{NIR} < 0.015\,\mathrm{Sr^{-1}}$	109	85.16	490	97.80
R_{RS} (765)/R_{RS} (400) < 0.700	109	85.16	468	93.41
R_{RS} (760)/R_{RS} (400) < 0.700	108	84.38	470	93.81
L_W (940)/L_W (460) < 0.090	108	84.38	488	97.41
R_{RS} (760)/R_{RS} (460) < 0.650	107	83.59	473	94.41

OSD

8, 613–638, 2011

Table 2. Summarised meteorological and sunglint flag conditions. The meteorological (Wernand, 2002) flags are represented by Flag 1–3. The sunglint flag can be implemented either as Flag 4a or Flag 4b depending on availability of measured water leaving radiance, L_W or remote sensing reflectance R_{RS}. For the flagging purposes of this study Flag 4a was implemented.

Flag name	Purpose	Test conditions
Flag 1	The "minimal flag" sets the lower limit for which significant incoming solar radiation can be measured.	E_S (480 nm) > 20 mW m^{-2} nm^{-1}.
Flag 2	The "shape flag" will mask optical measurements influenced by dusk "red colouring of the sky" or dawn radiation.	E_S (470 nm)/E_s (680 nm) > 1
Flag 3	The "rainfall flag" will mask optical measurements influenced by precipitation or high humidity.	E_S (940 nm)/E_s (370 nm) > 0.25
Flag 4a	The "sunglint flag" will mask optical measurements influence by sunglint based on L_W.	Mean L_W (700–950 nm) < 2 mW m^{-2} nm^{-1} Sr^{-1}
Flag 4b	Alternative "sunglint flag" based on R_{RS}.	Minimum $(R_{RS})_{NIR}$ < 0.010 Sr^{-1}

Discussion Paper | Discussion Paper | Discussion Paper | Discussion Paper |

OSD

8, 613–638, 2011

Quality control of automated hyperspectral measurements

S. P. Garaba et al.

Table 3. The percentage of sunglint free observations in relation to the azimuthal angle Φ_{derived}. These observations were obtained after filtering with the meteorological masks (Wernand, 2002).

Φ_{derived}	Number of observations collected at Φ_{derived}	Number of sunglint free observations at Φ_{derived}	%
$0^\circ < \Phi_{\text{derived}} \leq 45^\circ$	82	47	57
$45^\circ < \Phi_{\text{derived}} \leq 90^\circ$	48	26	54
$90^\circ < \Phi_{\text{derived}} \leq 135\circ$	107	89	83
$135^\circ < \Phi_{\text{derived}} \leq 180^\circ$	80	67	85
$180^\circ < \Phi_{\text{derived}} \leq 225^\circ$	56	52	94
$225^\circ < \Phi_{\text{derived}} \leq 270^\circ$	94	85	90
$270^\circ < \Phi_{\text{derived}} \leq 315^\circ$	87	76	87
$315^\circ < \Phi_{\text{derived}} \leq 360^\circ$	75	59	80
Total	629	501	

OSD
8, 613–638, 2011

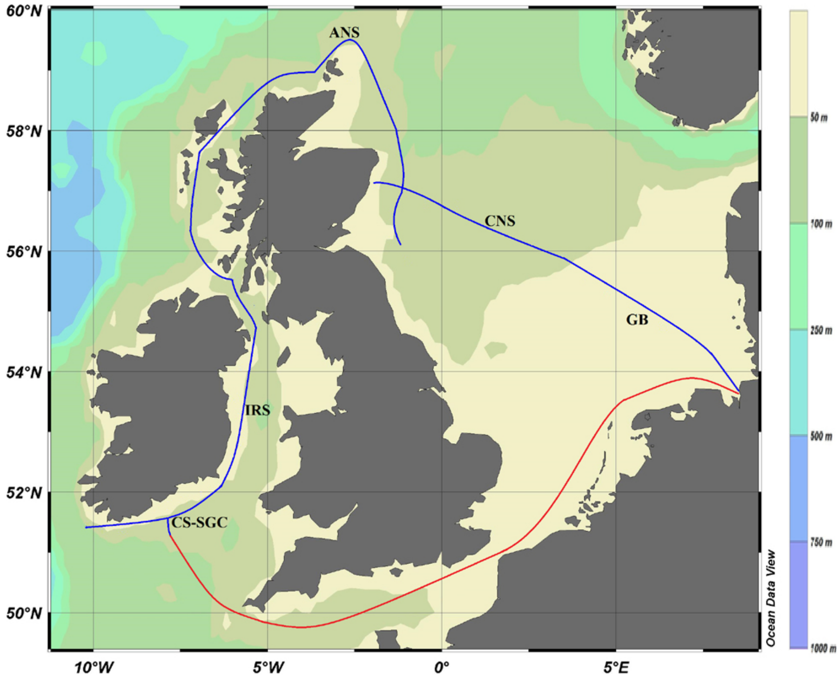

Fig. 1. R/V *Heincke* HE302 cruise track were above-water hyperspectral optical measurements were performed between 21 April and 14 May 2009. The blue line represents the track were optical measurements were collected, and the red line is for the return cruise to Bremerhaven without measurements. The annotated sites are; the German Bight (GB), the Central North Sea (CNS), Atlantic inflow into North Sea (ANS), Irish Sea (IRS), and the Celtic Sea–St. George's Channel (CS–SGC).

OSD
8, 613–638, 2011

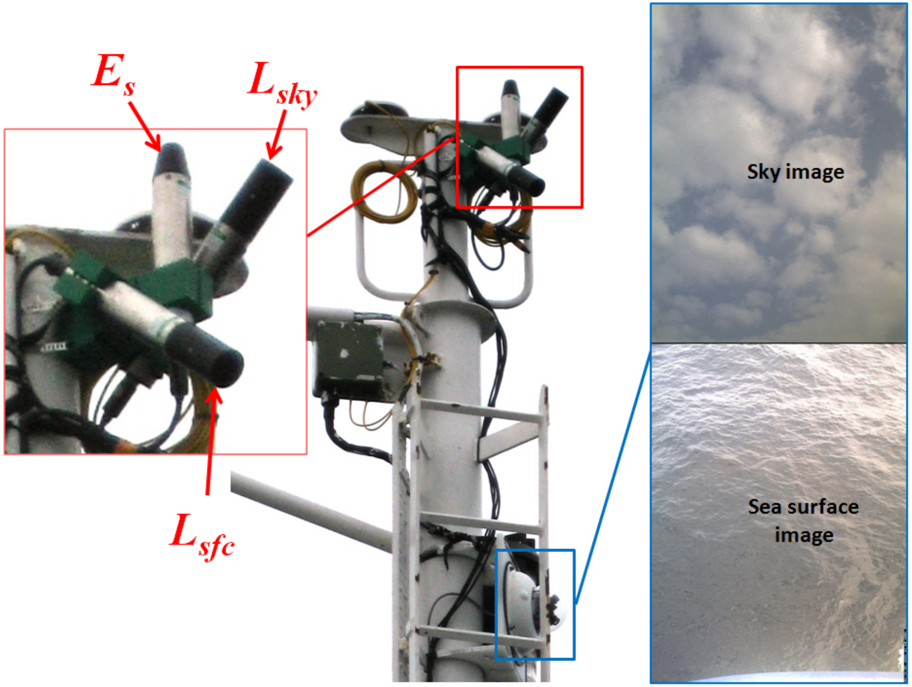

Fig. 2. The optical sensor and camera system setup. Highlighted in red on the left side is the RAMSES hyperspectral radiometers setup, and on the right side is the DualDome D12 camera system with a sample set of captured sky and sea surface images, not to scale.

OSD
8, 613–638, 2011

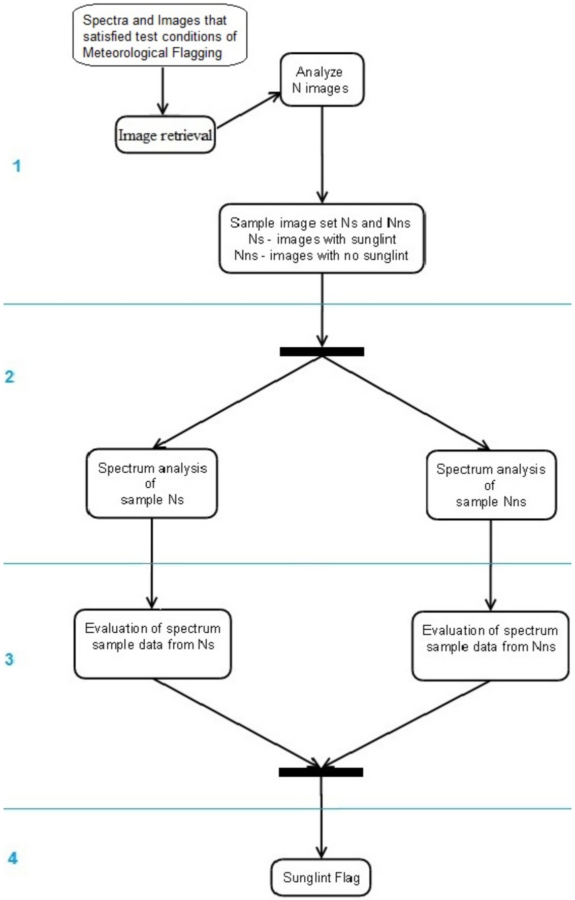

Fig. 3. A simplified activity diagram showing the 4 steps involved in generating the new sunglint flag. Please refer to the text for a detailed description of the individual steps.

OSD
8, 613–638, 2011

Quality control of automated hyperspectral measurements

S. P. Garaba et al.

Title Page
Abstract Introduction
Conclusions References
Tables Figures
Back Close
Full Screen / Esc
Printer-friendly Version
Interactive Discussion

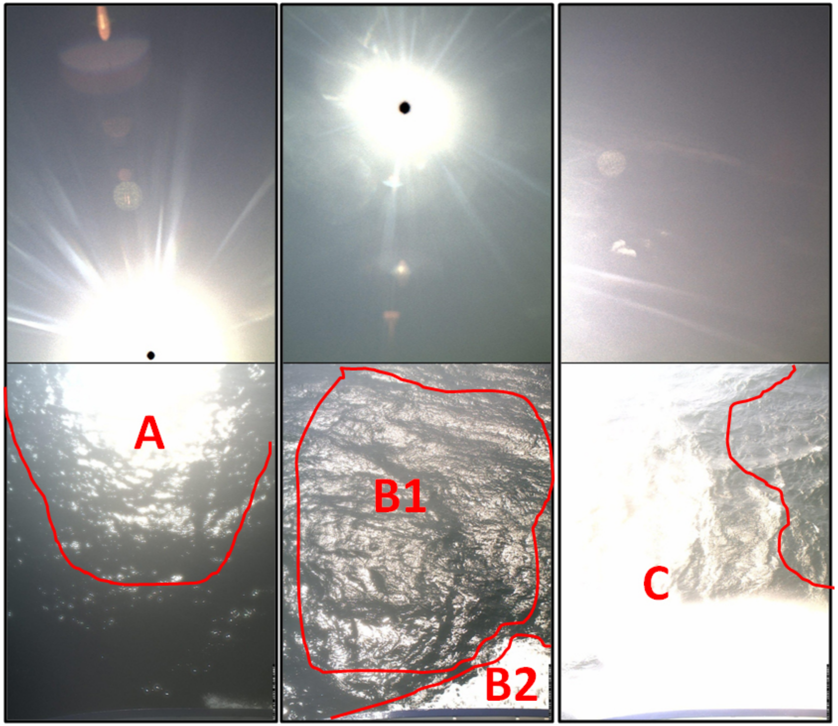

Fig. 4. Starboard side sky (top) and sea surface (bottom) images captured during R/V *Heincke* field campaign HE302 showing sources of erroneous measurements; A – sunglint, B1 – sunglint and B2 – whitecap or foam, and C – a combination of sunglint, whitecaps and foam.

OSD
8, 613–638, 2011

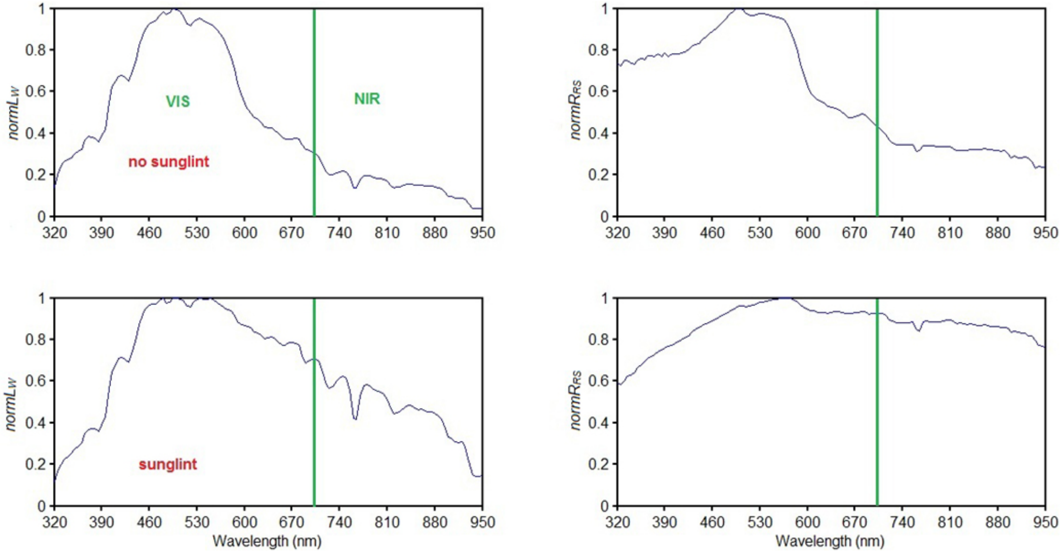

Fig. 5. Normalised mean spectral shapes for the sunglint free set Nns (top) and sunglint set Ns (bottom). The green line highlights the spectral limits for the VIS ($\lambda = 320$–700 nm) and NIR ($\lambda = 700$–950 nm). It shows that spectra affected by sunglint have normL_W and normR_{RS} enhanced in the NIR and slightly over the whole spectrum range, with respects to the sunglint free spectra.

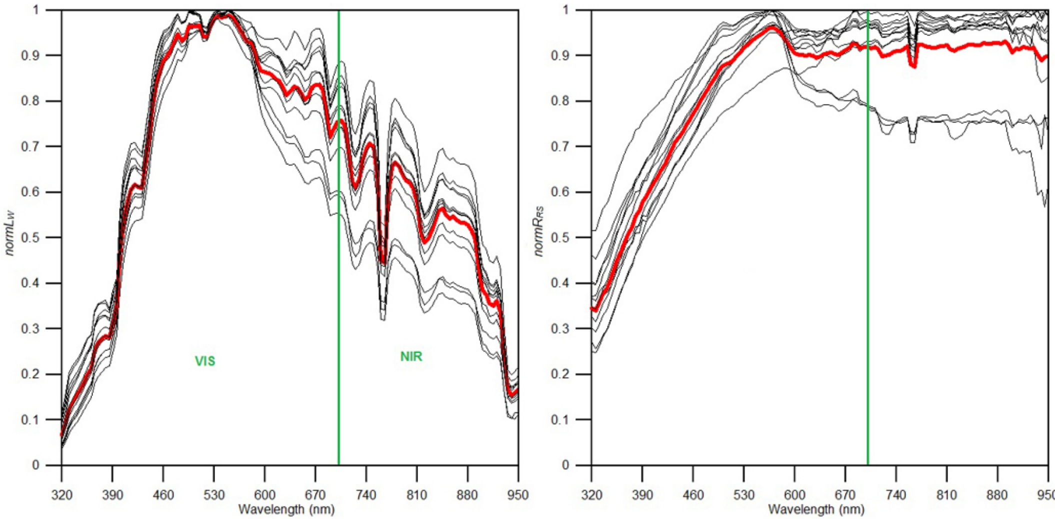

Fig. 6. 13 sample spectral shapes for sea surface images strongly affected by sunglint from the sunglint image set Ns. The red spectrum shows the mean spectra shape and the green line highlights the VIS and NIR spectral ranges.

OSD
8, 613–638, 2011

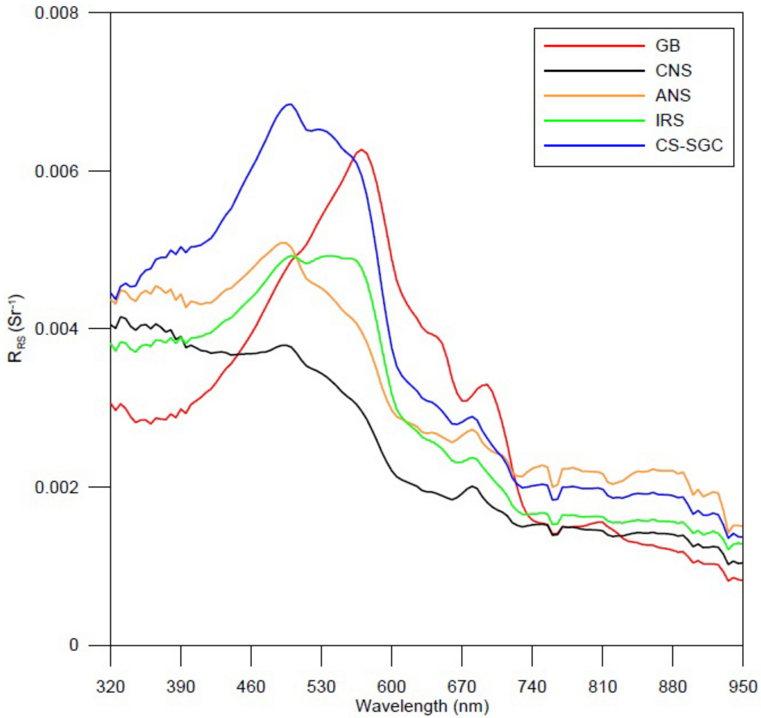

Fig. 7. Typical reflectance spectra from; the German Bight (GB), the Central North Sea (CNS), Atlantic inflow into North Sea (ANS), Irish Sea (IRS) and Celtic Sea–St. George's Channel (CS–SGC) collected during HE302 field campaign. These were filtered out as examples after applying the meteorological (Flag 1–3) and sunglint (Flag 4a) flagging from Table 2.

OSD
8, 613–638, 2011